Research Article Vol. 33, No. 7 / 7 Apr 2025 / Optics Express 14655
Optics EXPRESS

Sub-100 fε resolution strain sensing based on an optical fiber frequency comb

XINLONG LI, YONGQI LI, AND SHUN WU*

Hubei Key Laboratory of Optical Information and Pattern Recognition, Wuhan Institute of Technology, Wuhan 430205, China
*wushun@wit.edu.cn

Abstract: In this paper, we report a high-resolution optical fiber strain sensing system based on optical frequency comb (OFC) beat-frequency demodulation. This system enables both static and dynamic strain detection, featuring a large dynamic strain measurement range and a large spectral range. The sensor employed a fiber Fabry-Perot interferometer (FFPI) as the strain sensing element, which was probed by a narrow-linewidth laser stabilized to it. By leveraging the concept of beat frequency demodulation, the OFC, translated the optical frequency shifts within the strain sensor into the radio frequency (RF) for detection. Our findings revealed a static strain resolution of 247 pε, a dynamic strain resolution of 87 fε/Hz$^{1/2}$ at 8 kHz, and a large spectral range of 10 kHz, which enables it to be far away from low-frequency noise. Additionally, we investigated the potential of a free-running OFC with a stable repetition rate for high-resolution static strain sensing. By actively sweeping the OFC's offset frequency in conjunction with the FFPI, we achieved a static strain resolution of 630 pε. This sensor system offers high resolution, moderate cost, and a degree of portability, rendering it suitable for a range of geophysical research applications.

1. Introduction

High-resolution optical fiber strain sensing has received extensive attention in recent years due to its pivotal role in crustal strain monitoring [1,2], acoustic frequency detection above 10 Hz [3] and other areas. To capture rapid or high-frequency strain signals, such as those in underwater acoustic detection [4], the sensing system must possess the capability for dynamic strain detection. Moreover, the detection of low-frequency static strain is equally important for applications like low-frequency seismic monitoring and crustal deformation detection. Consequently, a sensing system equipped with both dynamic and static strain detection capabilities stand to gain significant advantages in the identification of various strain signals. Typically, the sensing system relies on strain-sensitive fiber Bragg gratings (FBGs), i.e., phase-shifted fiber gratings (π-FBGs) [5] and a FFPIs [6–9], as its primary sensing element [10–12]. These systems have achieved dynamic resolutions in the pε and sub-pε ranges [6]. However, these methods are primarily suited for characterizing dynamic strain, rather than static strain measurement. Specifically, while Ref. [6] achieves exceptional low-frequency noise performance (<100 Hz) suitable for static strain sensing, it exhibits two fundamental limitations: (1) inability to generate continuous RF-frequency outputs for real-time static strain monitoring, and (2) constrained dynamic detection bandwidth capped at ~1 kHz.

To achieve both high static and dynamic resolution, an acousto-optic modulator (AOM) is typically utilized to fine-tune the frequency of the source laser within a specified strain condition. Initially, the source laser's frequency is shifted by the AOM before being stabilized to the sensing element. When strain is applied to the sensing element, the resulting shift in the resonance frequency produced by the sensor prompts the AOM to adjust the laser frequency, ensuring that the laser remains locked to the sensing element. The minimum variation in the AOM's driving frequency corresponds to the minimum static strain that the system can resolve. In 2018, Zuyuan

#551796 https://doi.org/10.1364/OE.551796
Journal © 2025 Received 11 Dec 2024; revised 30 Jan 2025; accepted 19 Feb 2025; published 24 Mar 2025

Optics EXPRESS

He *et. al.* studied the strain sensor that employed a mode-locked laser (MLL) injected into two distributed feedback lasers (DFB-FLs) for wavelength multiplexing [13], based on AOM frequency shifting and Pound-Drever-Hall (PDH) [14] frequency stabilization. By demodulating the AOM frequencies of both the sensing and reference lasers, they achieved a static strain resolution of 72 pε within 100 seconds, with a dynamic resolution of 4 pε/Hz$^{1/2}$ at 30 Hz [14]. The following year, they further explored the injection locking between DFB-FLs and distributed Bragg reflector fiber lasers (DBR-FLs) for static strain detection, utilizing the same methodology. This led to an improved dynamic strain resolution of 0.58 pε/Hz$^{1/2}$ at a strain frequency of 1 kHz [15]. However, the static resolution of 248 pε was inferior to the 72 pε achieved in the earlier study. Although this method can detect both static and dynamic strains, the static strain detection range is quite limited (approximately 600~700 nε) due to the narrow bandwidth available for AOM frequency modulation.

An alternative approach for measuring static strain resolution involves utilizing the beat frequency [16,17] generated by two lasers: a sensing laser and a reference laser. The static strain resolution of the sensing system can be determined by analyzing the standard deviation of the radiofrequency (RF) beat frequency. In 2016, Wentao Zhang *et. al.* used the DFB-FL as a sensing laser, while a reference laser frequency-stabilized to a π-FBG. The frequency measurement of the RF heterodyne beat yielded a static strain resolution of 270 pε in 15 minutes, and a minimum dynamic strain resolution of 68 pε/Hz$^{1/2}$ from 1 Hz to 1 kHz [18]. This method translates the optical frequency shifts induced by external strain into a measurable RF frequency. However, this technique necessitates a precise control over the wavelength difference between the two continuous-wave (CW) lasers, which must be less than 8 pm to accommodate the photodiode (PD) with a 1 GHz detection bandwidth.

Optical frequency comb [19–24] stands out as a promising solution to resolve this problem. In recent years, the rapid development of fiber comb technology has led to the development of compact and less complex fiber comb systems, which are highly suitable for high-resolution strain sensing applications [6,7,25]. Provided that the wavelength of the CW laser falls within the optical bandwidth of the comb, an RF optical heterodyne beat at a frequency below the comb's repetition rate can always be produced, typically below 200 MHz.

In this letter, we proposed a FFPI fiber-optic strain sensing system based on an optical fiber frequency comb. With a repetition rate of 97 MHz, we readily achieve an optical heterodyne beat within the photodiode's detection range, obviating the need for precise frequency control of the CW sensing laser. To circumvent the limited detection range imposed by the AOM, we implemented a technique that stabilizes the CW laser to multiple cavity resonances. Critically, our approach enables the measurement of both static and dynamic strain with a static strain resolution of 247 pε and a minimum dynamic strain resolution of 87 fε/Hz$^{1/2}$. In addition, we introduced a measurement scheme using a half-stabilized comb. Our findings indicate that with only the repetition frequency stabilized, the OFC achieved a static strain resolution of 630 pε. We also discussed the measurement range of the sensing system in the face of sudden static strain and continuous dynamic strain. The results showed that the sensing system had a static and dynamic strain measurement range of 1080 nε and 950 με, respectively. Our research demonstrates that this sensor system offers high resolution, moderate cost, and a degree of portability, making it well-suited for a variety of geophysical research applications.

2. Experimental setup and principles

Figure 1 shows the experimental setup and principal diagram of the optical fiber strain sensing system. The sensing element fiber FFPI consisted of two FBGs (with center wavelength of 1539.4 nm) separated by 20 cm of single-mode fiber. Each FBG had a reflectivity of 95% with an optical bandwidth of 1 nm. The measured cavity linewidth was 11.9 MHz. A section of the FFPI is adhered to the PZT used to apply strain. The PZT has a maximum operating voltage of 150 V

Optics EXPRESS

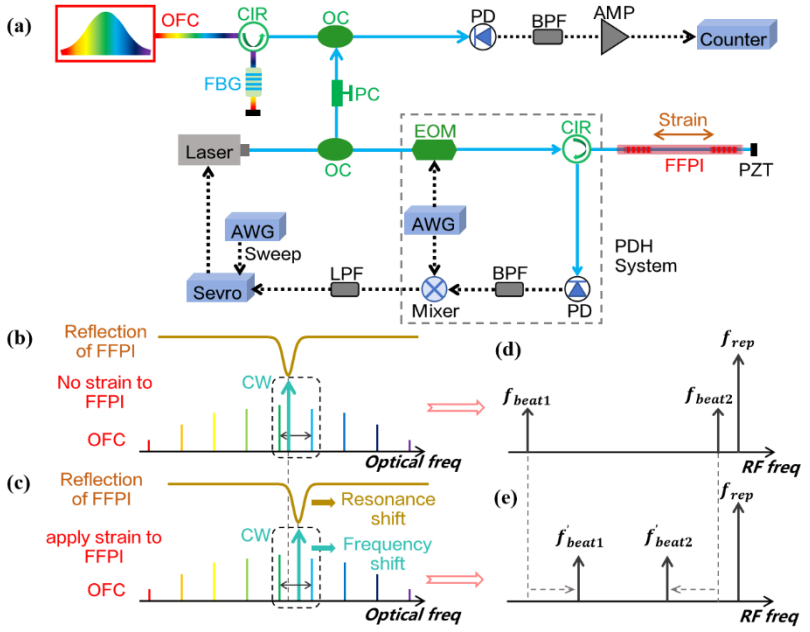

Fig. 1. (a) Schematic diagram of the optical fiber strain sensing system. (b-c) Principal diagram illustrating the optical heterodyne beat between the optical frequency comb (OFC) and the CW laser. (d), (e) Schematic diagram of the RF domain after beating frequency demodulation in the imaginary line of Figs. (b) and (c). CIR: circulator; FBG: Fiber Bragg Grating; OC: optical coupler; PC: polarization controller; EOM: electro-optic modulator; PD: Photodetector; BPF: band-pass filter; LPF: low-pass filter; AMP: amplifier; Counter: frequency counter; AWG: arbitrary waveform generator; Servo: Servo controller.

with a maximum extension of 9 μm, corresponding to an axial strain of 27με for FFPI. The FFPI was fixed and placed in a sealed insulation box to reduce environmental noise, and temperature effects. The sensing laser was a narrow-linewidth laser at around 1539.4 nm, frequency stabilized to the FFPI using PDH locking. An electro-optic modulator (EOM) was used to modulate the phase of the laser at a frequency of 60 MHz. The modulated light entered the FFPI through an optical circulator. The reflected light reached the photodetector (PD) and passed through a 0~32 MHz band-pass filter (BPF) before being converted into RF signal which carried the relative phase information between the frequency of the laser and the cavity. The bandwidth of the BPF was selected to avoid overlapping conjugate beatnote signals. The filterd RF signal was mixed with the EOM driving frequency and generated the error signal, which was fed back to the laser to achieve frequency stabilization under the action of servo electronics (Newport, LB1005). When the external axial strain was applied through a PZT attached to the FFPI, the laser frequency would always follow the shift of the cavity resonance. The optical response bandwidth of the CW sensing laser was found to be 34 kHz. The ultimate response bandwidth of the laser sensor was limited by the electrical response bandwidth of the PZT, which was measured to be 12.5 kHz.

The homemade OFC in Fig. 1(a) was a mode-lock laser (MLL) with a central wavelength of 1535 nm, and 3 dB optical bandwidth of 15 nm. The output of the OFC was filtered by a FBG before combining with the CW laser to perform the heterodyne beat on the PD. Figure 1(b-g) showed the principal diagram illustrating how the optical heterodyne beat frequency changes when an axial strain was applied to the FFPI. When the FFPI is not under strain action (Fig. 1(b)), the frequency of the CW laser was stabilized to the cavity resonance, representing by the brown curve. Therefore, a pair of optical heterodyne beat frequencies f_{beat1} and f_{beat2} were produced

Optics EXPRESS

and satisfy the condition of $f_{beat1} + f_{beat2} = f_{rep}$. The spectrum diagram is shown in Fig. 1(d). When the FFPI is subjected to the strain (Fig. 1(c)), the CW frequency followed the change of the cavity resonance. The beat frequency became f'_{beat1} and f'_{beat2}, as shown in Fig. 1(e). By using BPF to select one of the beat frequencies, the frequency change can be observed and recorded in real time in the frequency counter (Keysight, 53230A).

3. Experimental results

This section presents experimental results for characterizing both dynamic and static strain resolution performance. Since the external strain was applied to the FFPI in the axial direction, leading to the variation of the resonant frequency of the FFPI. As a result, the frequency of the CW sensing laser which stabilized to the FFPI through PDH locking changed accordingly. In this scheme on one hand, the dynamic strain resolution is solely measured by the strain power spectral density of the sensing laser, regardless of the fiber comb. On the other hand, static strain resolution is determined by the frequency stability of the optical heterodyne beatnote. In this section, we will firstly describe the experimental dynamic strain resolution measurement. Then we will discuss the static strain resolution performance using free-running and stabilized fiber comb.

3.1. Dynamic strain resolution measurement

Figure 2 illustrated the measurement results for stabilizing the CW sensing laser to the FFPI. The blue curve in Fig. 2(a) showed the PDH error signal and the corresponding resonance peak for the cavity transmission, plotted in red. The lock point of the optimized error signal was centered at zero volt with the frequency discrimination slope of 15 nV/Hz. When the laser was locked, the error signal continuously stayed at the lock point while the cavity exhibits maximum transmission, as shown in Fig. 2(b).

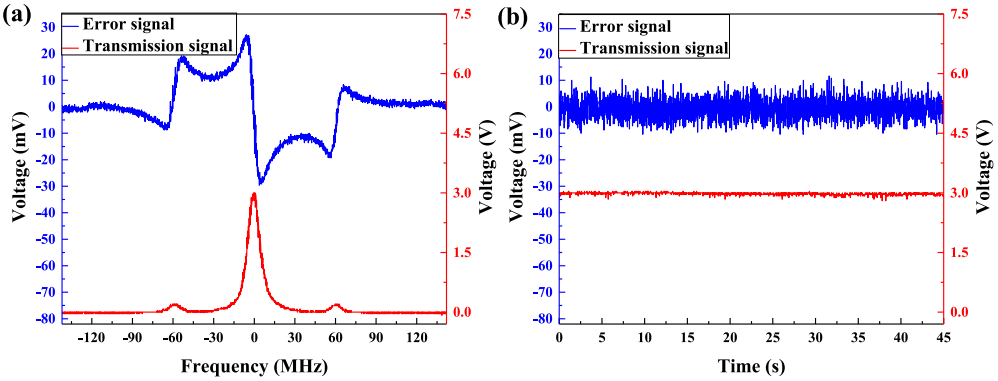

Fig. 2. (a) Error signal (blue) for laser stabilization to the FFPI, and transmission resonance (red) of the FFPI. The frequency discrimination slope of the error signal is 15 nV/Hz. (b) Near zero error signal and maximum transmission indicating that the laser was locked to the FFPI resonance.

When the laser was locked to the FFPI resonance, the dynamic strain of the sensor can be characterized by the strain power spectral density spectrum, expressed as the following [8]:

$$S_\varepsilon(f) = \frac{S_{\Delta\nu}(f)}{(\nu_B K)^2} = \frac{S_V(f)}{(\nu_B K D)^2}[\varepsilon^2/Hz] \tag{1}$$

Where ν_B is the Bragg frequency, K is the elastic constant of the fiber. For silica fiber, the normalized strain responsivity at constant temperature is about 0.78 ε^{-1} [26]. $S_V(f)$ is the power

Optics EXPRESS

spectral density of the error signal, D is the voltage frequency conversion coefficient, or the frequency discrimination slope of the error signal. $S_{\Delta\nu}(f)=S_V(f)/D^2$ is the power spectral density of the frequency fluctuation between the resonance frequency of the laser and the FFPI. The power spectral density of the error signal $S_V(f)$, dominated by $1/f$-noise [5], is influenced by both the laser's intrinsic linewidth and servo control parameters. Narrowing the laser linewidth suppresses low-frequency noise, while optimizing FBG reflectivity improves the FFPI's linewidth. Furthermore, increasing the frequency discrimination slope D amplifies the denominator term ($\nu_B KD$), effectively lowering $S_\varepsilon(f)$.

Figure 3 showed the strain power spectral density spectrum in the frequency range of 1 Hz ~ 10 kHz by the oscilloscope (Rohde&Schwarz, MXO-4). The large bandwidth enables suppression of low-frequency environmental noise while resolving high-frequency strain signals with enhanced signal-to-noise ratio (SNR). The black dotted line is the spectrum noise from the oscilloscope, which represents the limit of the spectrum noise of the signal that can be measured. The blue and red curves represented the strain power spectral density with and without strain signal applied to the FFPI, respectively. The blue peak frequency component at 8 kHz was caused by sinusoidal strain signal. The background strain power spectral density at 8 kHz is 7.5×10^{-27} ε^2/Hz, and the corresponding dynamic strain resolution can be calculated from its square root, with a value of 87 fε/Hz$^{1/2}$. The results show that the minimum strain that the sensing system can distinguish is 87 fε at the frequency of 8 kHz, which is better than the pε resolution in the work of [14,18,25]. In addition to this 8 kHz major frequency component, the spectrum also showed multiple spikes in the range of 30 Hz~1 kHz regardless of the strain. These spikes were caused by mechanical vibration or other environmental noise from the experimental platform. A large spectral range of 10 kHz enabled us to avoid low-frequency environmental noise and detect high- frequency strain signals with a higher SNR. Theoretically, the spectral range can be extended to the MHz order of magnitude by using lasers with a higher response bandwidth.

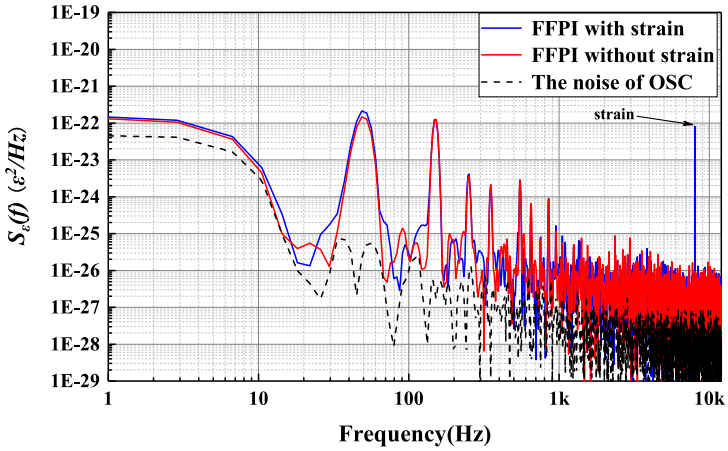

Fig. 3. Strain power spectral density of the 1539 nm laser locked to the FFPI with (blue solid) or without (red solid) strain. The black dotted curve represented the noise floor of the oscilloscope.

3.2. Static strain resolution measurement using f_{rep} stabilized fiber comb

The static resolution is determined by the ratio of the standard deviation of the beat frequency (SD) to the strain sensitivity (S) as follows,

$$R = SD/S \tag{2}$$

Optics EXPRESS

The static resolution is governed by the frequency stability of f_{beat}, which depends on the linewidth of the laser, the FFPI and the comb. A narrower laser linewidth reduces frequency jitter in the CW laser, while a smaller cavity linewidth or higher FBG reflectivity increases the frequency discrimination slope D, thereby improving f_{beat} stability. Additionally, using highly stable optical and radio-frequency references ensures robust performance of the comb.

As the first step of static strain measurement, we conducted the static strain measurement in our system using an OFC with stabilized repetition frequency and a free-running carrier-envelope offset frequency, as shown in Fig. 4. To weaken the slow frequency drift of the comb offset frequency f_{ceo}, we performed the measurement when the f_{ceo} was "swept" at a rate faster than the frequency of the slow drift. Figure 4(b) illustrates the principle of this "sweep measurement". During the time from 0 to t_1, we introduced a sinusoidal strain modulation on the PZT stretcher of the FFPI. The frequency of the CW sensing laser changed accordingly, with an amplitude of Δf_{CW}. Meanwhile, f_{ceo} was swept in phase with the strain modulation by sweeping the pump current of the OFC. The modulation amplitude of f_{ceo} was carefully tuned such that we were able to obtain a stable optical heterodyne beat f_{beat}, as shown in Fig. 4(c). This was performed in the following steps: with stabilized repetition rate, we characterized the dependence of optical heterodynene beat variation Δf_{beat} on the PZT modulation amplitude and pump current separately. Linear coefficients of 0.25 MHz/mV_{pp} (for PZT) and 0.05 MHz/mV_{pp} (for pump) were obtained, which enabled predictive compensation. The f_{beat} was continuously monitored via a frequency counter. Precise adjustment of both pump current and PZT modulation amplitudes, along with their relative phase, enabled stabilization of f_{beat}. In other words, the comb movement was compensated by sweeping the f_{ceo}. So the static strain resolution of the sensing system can be reflected from the standard deviation of f_{beat}. From time t_1 to t_2, as we further increased the modulation amplitude of the FFPI-PZT while the f_{ceo} scan remained unchanged, Δf_{CW} became larger. Therefore, since the change amplitude of f_{CW} is greater than that of f_{ceo}, the beatnote signal begins to produce periodic oscillations. In this case, Δf_{beat} was introduced entirely by the PZT modulation, regardless of the comb movement. Therefore, the strain sensitivity of the FFPI can be calculated from the oscillation amplitude Δf_{beat}.

Figure 5(a) presents experimental measurement of Δf_{beat} over a 20-second duration. During the first 10 seconds, concurrent 2 Hz sinusoidal modulation was applied to both the optical frequency comb's pump current and the FFPI's PZT stretcher, yielding a beatnote standard deviation of 84.9 kHz (inset). Subsequent modulation enhancement of the PZT stretcher to 220 mV_{pp}, equivalent to 37.1 nε, induced systematic 5 MHz periodic oscillations in f_{beat}. The observed discontinuities in the sinusoidal beat frequency traces arise from periodic dead-time intervals inherent to the frequency counter's sampling protocol. The dynamic strain sensitivity can be calculated from $\Delta f_{beat}/\Delta\varepsilon$ as 134.7 MHz/με. Therefore, based on Eqn (2), the static resolution (SD/S) can be calculated as 630 pε.

Comparative experiments without f_{ceo} sweeping via pump modulation reveal critical performance contrasts, as shown in Fig. 5(b). During the initial 10 seconds, with f_{ceo} in uncompensated free-running state, slow frequency drift emerged in f_{beat}, exhibiting 1.3 MHz peak-to-peak variation with standard deviation of 317.1 kHz, corresponding to 2354 pε static resolution. Subsequent PZT modulation (10-20 s interval) failed to eliminate the inherent drift. This result demonstrates a 3.7-fold enhancement in beatnote stability (630 pε vs. 2354 pε) through active f_{ceo} sweeping, confirming its effectiveness in static strain measurement.

During the measurement, we noticed that the f_{rep} stabilization was influenced as we swept the pump current due to the dependence of the refractive index for the laser cavity on the pump power [27]. Consequently, the frequency stability of f_{beat} from 0 to t_1 time experienced deterioration. Figure 5(c) shows the f_{rep} stabilization measurement with and without the sweep for 0.05 s sampling time. The Allan deviation (AD) of f_{rep} was reduced from 8.71 mHz to 5.18 mHz by a factor of 1.68 when the sweep was off. To optimize the sweeping conditions with minimal impact

Optics EXPRESS

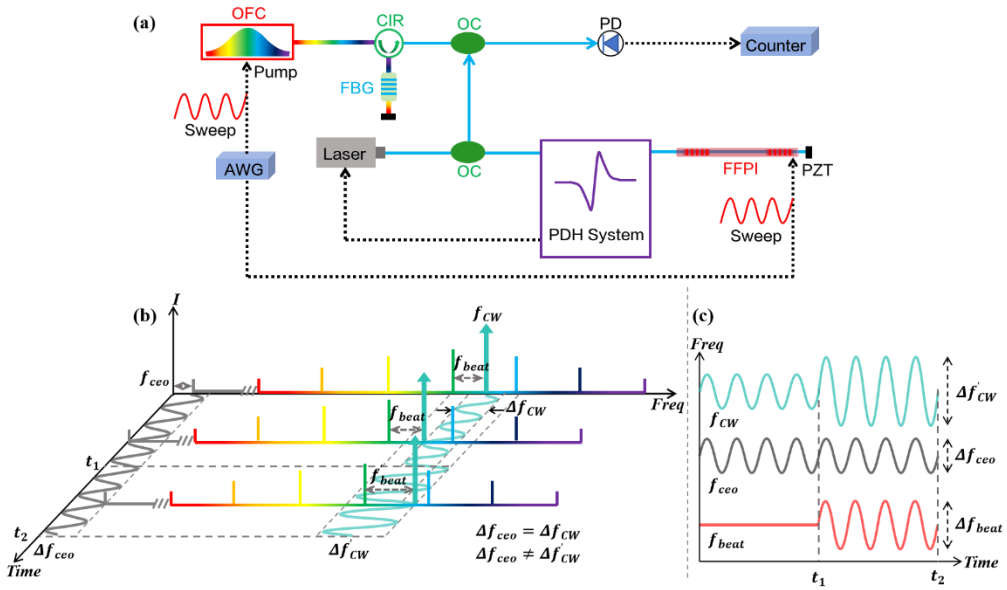

Fig. 4. Strain sensing principle using the "sweep frequency" method based on an optical comb with stabilized repetition frequency and free-running carrier-envelope offset frequency (f_{ceo}). (a) The schematic diagram of the "sweep frequency" method for static strain resolution measurement. (b-c) The illustrating diagram showing the principle of the "sweep frequency" method. From time 0 to t_1, the pump current was swept with an appropriate amplitude such that the f_{ceo} followed the frequency change of the CW laser, and a stable beat frequency (f_{beat}) was obtained. From t_1 to t_2, the strain modulation amplitude increases.

on the frequency stability of f_{beat}, we tested a range of pump current modulation amplitudes. Specifically, we characterized the ratio of the ADs with and without the sweep, as well as achieving a minimized static resolution. Figure 6 represented the measured AD ratio and static resolution under various sweeping amplitudes. The data show that as the sweep amplitude for f_{rep} was decreased from 30 mV_{pp} to 10 mV_{pp}, the stability of f_{beat} was enhanced, as evidenced by the reduction in the AD ratio from 9.16 to 1.68 indicated by the black diamonds in Fig. 6. Meanwhile, the static strain resolution was also reduced from 1387 pε to a minimum value of 630 pε, as represented by the red stars.

However, further reduction in the sweep amplitude below 10 mV_{pp} eventually resulted in a decline in the static strain resolution, as shown in Fig. 6. When the sweep amplitude of f_{ceo} was sufficiently large compared to the frequency drift of a free-running f_{ceo}, while the CW laser was modulated in phase with the f_{ceo}, a relatively stable f_{beat} was achievable. However, if the sweep amplitude was diminished to a level where the frequency drift of a free running f_{ceo} could no longer be overlooked, the stability of f_{beat} would notably deteriorate. Based on the above discussions and measurements presented, an optimized sweep amplitude of 10 mV_{pp} was determined to achieve a static strain resolution of 630 pε with a free-running OFC. Our approach provides a solution for high resolution fiber strain sensing using a free-running OFC.

3.3. *Static strain resolution measurement using a fully stabilized fiber comb*

In this section, we performed the same static strain resolution experiments using a fully stabilized homemade OFC [28]. The repetition rate of the comb f_{rep} was 97.36 MHz and stabilized to the GPS-disciplined Rb oscillator, while the offset frequency was stabilized by locking one of the comb teeth to the P (16) overtone transition line (~1542.4 nm) of acetylene gas ($^{13}C_2H_2$).

Optics EXPRESS

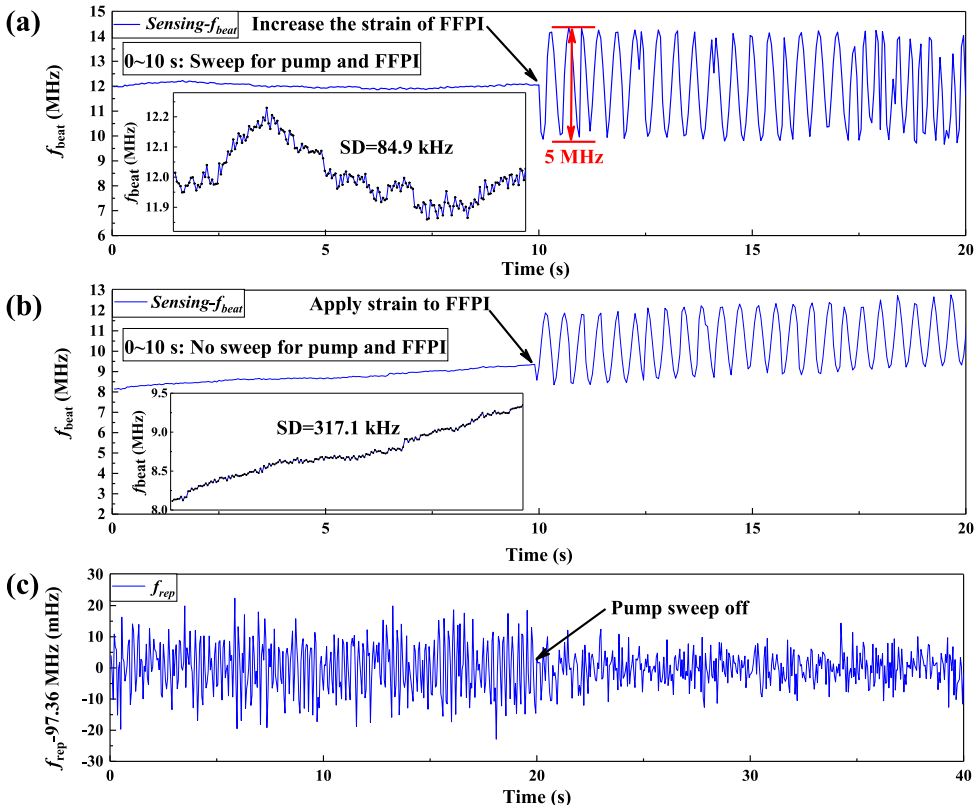

Fig. 5. (a) Real-time measurement of the beat frequency obtained by "sweeping frequency" method in 0 to 20 s. (b) Real-time measurement of the beat frequency obtained without using the "sweeping frequency" method in 0 to 20 s. (c) Real-time variation of the repetition frequency when the sweep of the pump source was on (0 ~ 20 s) and off (20 ~ 40 s).

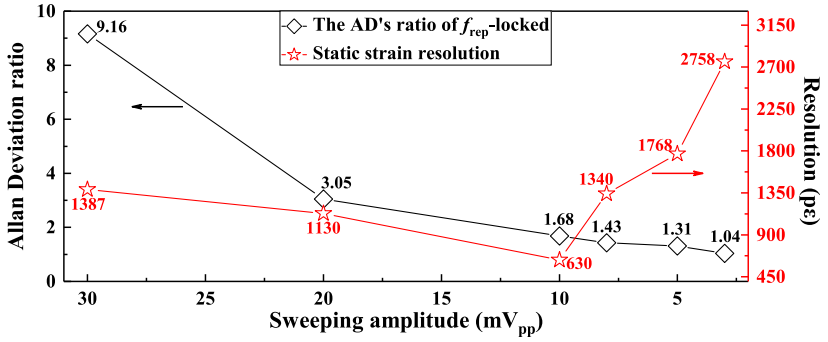

Fig. 6. The ratio (black diamond) of the Allan Deviations with and without sweeping the pump current while f_{rep} was locked. The static strain resolution (red star) under different sweeping amplitudes.

Optics EXPRESS

Figure 7 showed the stability measurement of f_{rep} and f_{beat} recorded by the frequency counter within 25 min at 1 s sampling time. The Allan deviation of f_{rep} and fbeat were measured to be 0.38 mHz and 3.2 kHz, respectively, corresponding to a fractional instability of 4.0×10^{-12} and 1.7×10^{-11} at 1 s.

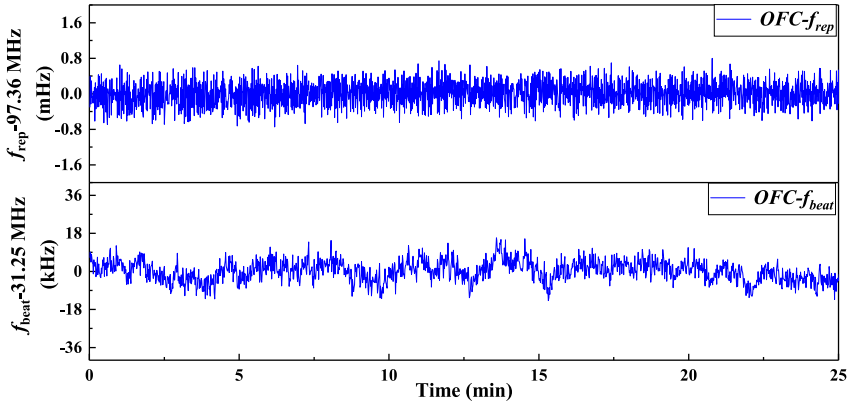

Fig. 7. Locking results of the optical comb sensing system within 25 min under 1 s sampling time. (a) Stabilized repetition frequency. (b) Stabilized optical heterodyne beat frequency between the optical comb and the CW laser locked to the P (16) absorption line of acetylene gas ($^{13}C_2H_2$).

When we performed the optical heterodyne beat between the fully stabilized fiber comb and the sensing laser, an RF heterodyne beatnote denoted as *Sensing-*f_{beat} was obtained. Figure 8 showed the measurement of *Sensing-*f_{beat} with and without a sinusoidal strain signal applied to the sensing laser, respectively When we applied a 3 Hz sinusoidal strain signal with amplitude corresponding to 55 nε to the FFPI-PZT, the *Sensing-*f_{beat} followed the strain modulation exhibiting a peak-to-peak amplitude of 7.4 MHz, as shown in Fig. 8(a). According to this result, the strain sensitivity was calculated to be 134.5 MHz/με. When no strain was applied, a stable *Sensing-*f_{beat} was obtained as shown in Fig. 8(b), with standard deviation of 33.3 kHz, corresponding to a static strain resolution of 247 pε. Compared to measurement performed using a free-running comb in Fig. 5, the static resolution using a fully stabilized comb was improved by a factor of 2.5 due to better frequency stability of the comb.

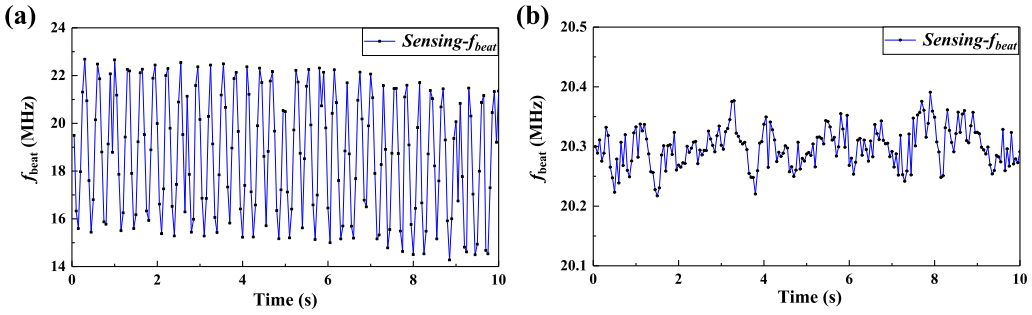

Fig. 8. Measurement of the optical heterodyne beat frequency (*Sensing-*f_{beat}) within 10 s: (a) under sinusoidal strain modulation (3 Hz, 55 nε), and (b) without sinusoidal strain modulation.

Here, we discuss the impact of temperature change to the sensing FFPI. The resonance frequency of the FFPI was not only linearly responsive to axial strain but also to temperature

Optics EXPRESS

changes. For the FFPI with a center wavelength of 1539 nm, the theoretical laser frequency shift is calculated to be 1.25 GHz/°C [29]. Therefore, as temperature changes, the sensing beat frequency drift correspondingly, leading to a degradation in the static strain resolution. Beyond encapsulation in protective housings, one could integrate active temperature stabilization systems within the sensor packaging, or embed the sensor in vibration-damping media such as sand beds or specialized viscoelastic composites. By effectively attenuate low-frequency environmental perturbations induced by temperature variation, acoustic vibration or turbulent airflow interactions, our device should be able to achieve sub-nε static strain resolution.

4. Discussion

In this section, we shall discuss the detection range in two schemes: static and dynamic strain measurements. The static strain detection range refers to the maximum locking range when the static system remains locked as a sudden large strain is applied. In this case, our system is mainly limited by the CW locking to the FFPI. To investigate the maximum CW locking range, we applied an instantaneous non-zero DC voltage representing a large strain, to the FFPI-PZT. Figure 9(a) was an example of this test. The CW laser initially stayed locked when the FFPI exhibited a maximum transmission (red trace), and a stable error signal was obtained (blue trace). Then at 25 seconds, the CW laser went out of lock due to the sudden external strain applied to the FFPI. We recorded whether the CW laser remained locked when eight different voltages were applied. The results were shown in Fig. 9(b), where the blue squares and red triangles represented "locked" or "out of lock", respectively. Each experiment was repeated ten times. We considered 5.82 V was the maximum DC voltage under which the CW laser could mostly remain locked, which corresponded to a strain of 1080.36 nε. This result also suggested that our system was capable of withstanding environmental vibrations that induced an axial strain of up to 1080 nε. To detect the beat frequency when a sudden strain is applied to the system, causing f_{beat} to jump abruptly by several "jump points", we can calculate the number of comb modes involved in the heterodyne beat before (n) and after (n') the sudden strain occurs [30]. By comparing n' with n, we can ascertain the number of repetition frequencies that the f_{beat} signal has traversed.

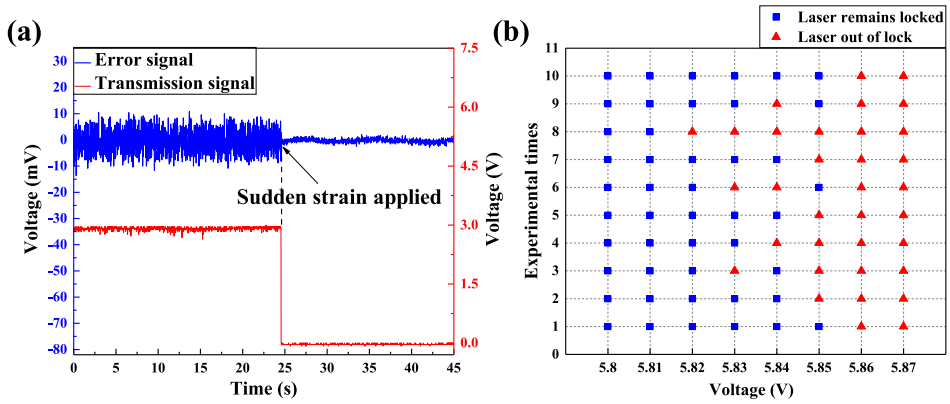

Fig. 9. (a) The error signal (blue) and cavity transmission (red) of the sensing CW laser when the laser was locked (0~24 s) and out of lock when a large strain was suddenly applied to the FFPI (24~45 s). (b) Statistical data of 80 sets for static strain limit range tests. Blue squares and red triangle indicated that the laser either remained locked or out of lock, respectively.

As for the dynamic detection range, it refers to the maximum locking range when the system stays locked as a continuously increasing strain signal is applied. The detection range of dynamic

Optics EXPRESS

strain is mainly limited by the frequency tuning range of CW laser and the bandwidth of FFPI, which is about 10 GHz (0.08 nm), and 125 GHz (1 nm), respectively. Once the strain gradually becomes large and the frequency deviation exceeds the tuning range of the laser, the laser frequency will jump one FSR and lock in the nearby laser resonance. Therefore, the dynamic strain detection range determined by the bandwidth of FFPI is about 925 με. Dynamic continuous strain greater than half of f_{rep} (corresponding to 362 nε) can be determined by the following method: Two distinct frequency counters can be employed. Each will be dedicated to monitoring one of the conjugate beat frequencies concurrently. This approach allows us to capture the "jump points" through both frequency counters. By tallying the number of jump points, we can determine how many times f_{beat} surpasses $f_{rep}/2$ throughout the entire process.

Table 1. Performance comparison with others works

Reference	Light source	Strain sensor	Static resolution	Dynamic resolution	The maximum range of strain	Sensing scheme
[32]	CW	DFB-FL	——	10 pε/Hz$^{1/2}$@0.6 kHz	About 981 nε	AOM frequency shift
[14]	MLL	DFB-FL	72 pε	4 pε/Hz$^{1/2}$@30 Hz	About 706 nε	AOM frequency shift
[15]	DFB-FL	DBR-FL	248 pε	0.58 pε/Hz$^{1/2}$@1 kHz	About 100 με	AOM frequency shift
[25]	OFC	FFPI	90 pε	3 pε/Hz$^{1/2}$@1 kHz	About 610 nε	AOM frequency shift
[31]	CW	FFPI	——	14 fε/Hz$^{1/2}$@1 kHz	About 800 με	AOM frequency shift
[33]	CW	FFPI	——	1 fε/Hz$^{1/2}$@100 kHz	——	AOM frequency shift
[18]	**DFB-FL**, CW	DFB-FL	270 pε	67.8 pε/Hz$^{1/2}$@1 kHz	About 8 με	Beat frequency demodulation
Our work	OFC, **CW**	FFPI	247 pε	87 fε/Hz$^{1/2}$@8 kHz	About 925 με	Beat frequency demodulation

Then we compared our work with the performance of other high-resolution strain sensors in recent published literature, as shown in Table 1. The dynamic resolution of the strain sensor is primarily determined by the noise level of the laser source. Most studies listed here utilize CW lasers, with a few employing OFCs. The highest dynamic resolution at 1 kHz, as shown in Table 1, was achieved using a narrow-linewidth laser stabilized by an optical ultra-stable cavity (OUC) with a finesse of 600,000 [31]. While this method achieved a remarkable dynamic strain resolution of 14 fε/Hz$^{1/2}$, the use of the OUC to suppress laser noise significantly increased system complexity and cost. In contrast, our approach avoids such costly stabilization techniques, yet still achieves a competitive dynamic strain resolution of 87 fε/Hz$^{1/2}$ and a broad strain spectral range of up to 10 kHz. This demonstrates the effectiveness of our system in balancing performance and practicality. In addition, the work in Ref. [33] reported a dynamic resolution of 1 fε and a strain spectral range up to 100 kHz, achieved through active noise compensation via an acousto-optic modulator (AOM) in one arm of a Mach-Zehnder interferometer. However, this approach sustains fε resolution only for short-term measurements (minutes) and cannot resolve static strain. The sensing mechanisms in Table 1 are primarily based on either the "AOM frequency shift" or the "frequency demodulation" for optical heterodyne beat detection. Our work belongs to the latter. While the AOM frequency shift approach, which utilizes a single light source, such as OFC [25] or MLL, and employs temperature compensation [14] to achieve higher static resolution, it typically constrains the strain detection range due to the AOM's limited tuning range [14,25,32]. References [15] and [31] expanded the detection range to 100 με and 800 με,

Optics EXPRESS

respectively, by stabilizing the laser to adjacent resonances. As for the "frequency demodulation" method, we are the first to use OFC for the strain sensing demodulation, enabling both static and dynamic measurements. Our study, as referenced in Table 1, stands out with the broadest dynamic strain detection range, reaching up to 925 με. Furthermore, we have also presented a static strain measurement range of 1080 nε in response to sudden strain, an aspect that has not been documented in any of the works listed in Table 1. In summary, our strain sensing system is capable of both static and dynamic strain detection, characterized by high resolution and ease of measurement, which holds promising applications in the domain of geophysical research.

5. Conclusion

In conclusion, we proposed a high-resolution strain sensing system using OFC detection, allowing for both static and dynamic strain detection measurements. To the best of our knowledge, we are the first to use OFC for strain sensing demodulation, enabling both static and dynamic measurements. Our experimental results demonstrated a dynamic strain resolution of 87 fε/Hz$^{1/2}$ with 8 kHz dynamic bandwidth. With a fully stabilized OFC, the static strain resolution was measured to be 247 pε. Additionally, we introduced a measurement scheme employing a half-stabilized OFC, where locking only the repetition frequency yielded a static strain resolution of 630 pε. Finally, we discuss the measurement range of the sensing system in the face of sudden static strain and continuous dynamic strain. Compared to other fiber sensing systems [31,25], which rely on ultra-stable cavities or conventional comb stabilization configuration that generate f_{ceo} through an octave-spanning spectrum, our approach only employed a fiber cell for optical frequency stabilization. We believe that with the further development of miniaturized OFCs, our work offers a modest contribution to the advancement of high-resolution sensing applications in the field of OFCs for geophysical research, including the monitoring of crustal deformation and the observation of seismic activities.

Funding. Campus Science Foundation of Wuhan Institute of Technology (22QD01); Natural Science Foundation of Hubei Province (2023AFB778).

Acknowledgement. None.

Disclosures. The authors declare no conflicts of interest.

Data availability. Data underlying the results presented in this paper are not publicly available at this time but may be obtained from the authors upon reasonable request.

References

1. Q. Liu, Z. He, and T. Tokunaga, "Sensing the earth crustal deformation with nano-strain resolution fiber-optic sensors," Opt. Express **23**(11), 428–436 (2015).
2. Q. Liu, T. Tokunaga, K. Mogi, *et al.*, "Ultrahigh resolution multiplexed fiber Bragg grating sensor for crustal strain monitoring," IEEE Photonics J. **4**(3), 996–1003 (2012).
3. S. B. Foster, G. A. Cranch, J. Harrison, *et al.*, "Distributed feedback fiber laser strain sensor technology," J. Lightwave Technol. **35**(16), 3514–3530 (2017).
4. M. Moccia, M. Consales, A. Iadicicco, *et al.*, "Resonant hydrophones based on coated fiber Bragg gratings," J. Lightwave Technol. **30**(15), 2472–2481 (2012).
5. D. Gatti, G. Galzerano, D. Janner, *et al.*, "Fiber strain sensor based on a π-phase-shifted Bragg grating and the Pound-Drever-Hall technique," Opt. Express **16**(3), 1945–1950 (2008).
6. G. Gagliardi, M. Salza, S. Avino, *et al.*, "Probing the ultimate limit of fiber-optic strain sensing," Science **330**(6007), 1081–1084 (2010).
7. J. D. C. Jones, G. Gagliardi, M. Salza, *et al.*, "Optical-frequency-comb stabilized lasers for interrogation of fibre-resonator strain sensors," *in 20th International Conference on Optical Fibre Sensors*, 530–533 (2009).
8. Q. Liu, S. Zhao, and Z. He, "Improved Pound-Drever-Hall techniques for high resolution optical fiber grating sensors," J. Lightwave Technol. **39**(12), 3846–3854 (2021).
9. T. Yoshino, K. Kurosawa, K. Itoh, *et al.*, "Fiber-optic Fabry-Perot interferometer and its sensor applications," IEEE Trans. Microwave Theory Tech. **30**(10), 1612–1621 (1982).
10. J. Chen, Q. Liu, X. Fan, *et al.*, "Ultrahigh resolution optical fiber strain sensor using dual Pound-Drever-Hall feedback loops," Opt. Lett. **41**(5), 1066–1069 (2016).

Optics EXPRESS

11. C. Ghosh and V. Priye, "Augmentation of sensitivity of FBG strain sensor for biomedical operation," Appl. Opt. **57**(24), 6906–6910 (2018).
12. G. Gagliardi, S. De Nicola, P. Ferraro, *et al.*, "Interrogation of fiber Bragg-grating resonators by polarization-spectroscopy laser-frequency locking," Opt. Express **15**(7), 3715–3728 (2007).
13. S. Zhao, Q. Liu, J. Chen, *et al.*, "Pico-strain resolution multiplexed fiber grating sensor array interrogated with mode-locked laser," J. Lightwave Technol. **37**(18), 4838–4843 (2019).
14. E. D. Black, "An introduction to Pound-Drever-Hall laser frequency stabilization," Am. J. Phys. **69**(1), 79–87 (2001).
15. S. Zhao, Q. Liu, J. Chen, *et al.*, "Realization of sub-nano-strain static resolution with injection-locking between two fiber laser sensors," J. Lightwave Technol. **37**(13), 3166–3172 (2019).
16. B.-O. Guan, Y.-N. Tan, and H.-Y. Tam, "Dual polarization fiber grating laser hydrophone," Opt. Express **17**(22), 19544–19550 (2009).
17. O. Hadeler, M. Ibsen, and M. N. Zervas, "Distributed-feedback fiber laser sensor for simultaneous strain and temperature measurements operating in the radio-frequency domain," Appl. Opt. **40**(19), 3169–3175 (2001).
18. W. Huang, S. Feng, W. Zhang, *et al.*, "DFB fiber laser static strain sensor based on beat frequency interrogation with a reference fiber laser locked to a FBG resonator," Opt. Express **24**(11), 12321–12329 (2016).
19. H. Leopardi, J. Davila-Rodriguez, F. Quinlan, *et al.*, "Single-branch Er:fiber frequency comb for precision optical metrology with 10ˆ−18 fractional instability," Optica **4**(8), 879–885 (2017).
20. Y. Liu, Y. Guo, and S. Wu, "Frequency measurement of microwave signals in a wide frequency range based on an optical frequency comb and channelization method," Appl. Opt. **61**(13), 3663–3670 (2022).
21. L. C. Sinclair, I. Coddington, W. C. Swann, *et al.*, "Operation of an optically coherent frequency comb outside the metrology lab," Opt. Express **22**(6), 6996–7006 (2014).
22. H. Tian, R. Zhu, R. Li, *et al.*, "Broadband, high-power optical frequency combs covering visible to near-infrared spectral range," Opt. Lett. **49**(3), 538–541 (2024).
23. E. Russell, A. A. Ruth, B. Corbett, *et al.*, "Tunable dual optical frequency comb at 2 µm for CO_2 sensing," Opt. Express **31**(4), 6304–6313 (2023).
24. D. Laumer, S. Salman, Y. Ma, *et al.*, "Sub-Hz relative linewidths from an interferometrically stabilized mid-infrared frequency comb," Opt. Lett. **48**(11), 3055–3058 (2023).
25. S. Zhao, Q. Liu, and Z. He, "Multi-Tone Pound-Drever-Hall Technique for High-Resolution Multiplexed Fabry-Perot Resonator Sensors," J. Lightwave Technol. **38**(22), 6379–6384 (2020).
26. A. D. Kersey, M. A. Davis, H. J. Patrick, *et al.*, "Fiber grating sensors," J. Lightwave Technol. **15**(8), 1442–1463 (1997).
27. P. Yan, H. Hu, Z. Li, *et al.*, "Optical high repetition rate stabilization based an all-polarization-maintaining figure-of-nine Er-fiber laser," Opt. Commun. **513**, 128081 (2022).
28. Y. Li, X. Hu, H. Cheng, *et al.*, "All-fiber acetylene-referenced optical frequency comb," Opt. Commun. **531**, 129233 (2023).
29. G. Li, L. Ji, G. Li, *et al.*, "High-resolution and large-dynamic-range temperature sensor using fiber Bragg grating Fabry-Pérot cavity," Opt. Express **29**(12), 18523–18529 (2021).
30. K. Knabe, S. Wu, J. Lim, *et al.*, "10 kHz accuracy of an optical frequency reference based on $^{12}C_2H_2$-filled large-core kagome photonic crystal fibers," Opt. Express **17**(18), 16017–16026 (2009).
31. S. Zhao, Q. Liu, J. Chen, *et al.*, "Resonant fiber-optic strain and temperature sensor achieving thermal-noise-limit resolution," Opt. Express **29**(2), 1870–1878 (2021).
32. S. Zhao, Q. Liu, J. Chen, *et al.*, "Pε-resolution fiber grating sensor with adjustable measurement range and ultralow probe power," IEEE Photonics Technol. Lett. **31**(1), 19–22 (2019).
33. N. M. R. Hoque and L. Duan, "A Mach-Zehnder Fabry-Perot hybrid fiber-optic interferometer operating at thethermal noise limit," Sci. Rep. **12**(1), 12130 (2022).